Science Advances

AAAS

advances.sciencemag.org/cgi/content/full/1/9/e1500852/DC1

Supplementary Materials for

Lunar impact basins revealed by Gravity Recovery and Interior Laboratory measurements

Gregory A. Neumann, Maria T. Zuber, Mark A. Wieczorek, James W. Head, David M. H. Baker, Sean C. Solomon, David E. Smith, Frank G. Lemoine, Erwan Mazarico, Terence J. Sabaka, Sander J. Goossens, H. Jay Melosh, Roger J. Phillips, Sami W. Asmar, Alexander S. Konopliv, James G. Williams, Michael M. Sori, Jason M. Soderblom, Katarina Miljković, Jeffrey C. Andrews-Hanna, Francis Nimmo, Walter S. Kiefer

Published 30 October 2015, *Sci. Adv.* **1**, e1500852 (2015)
DOI: 10.1126/sciadv.1500852

The PDF file includes:

Supplementary Text
Morphology and morphometry of impact basins
Maps of impact basins
Multiring basins
Peak-ring basins and other sizeable lunar impacts
Basins without measurable rings that are identifed by GRAIL Bouguer gravity anomaly
Fig. S1. Serenitatis, Serenitatis North, and Lamont.
Fig. S2. Fitzgerald-Jackson.
Fig. S3. Amundsen-Ganswindt and Schrödinger.
Fig. S4. Nectaris and Asperitatis.
Fig. S5. Lorentz and Bartels-Voskresenskiy.
Fig. S6. Copernicus-H and Aestuum.
Fig. S7. Orientale and Orientale Southwest.
Fig. S8. Mendel-Rydberg.
Fig. S9. Imbrium and Iridum.
Fig. S10. Crisium and Crisium East.
Fig. S11. Humorum.
Fig. S12. Hertzsprung.
Fig. S13. Humboldtianum and Bel'kovich.
Fig. S14. Coulomb-Sarton and Fowler-Charlier.
Fig. S15. Smythii and Balmer-Kapteyn.

Fig. S16. Moscoviense and Moscoviense North.
Fig. S17. TOPO-22.
Fig. S18. Australe North.
Table S1. Lunar craters <200 km in diameter suggested from LOLA data.
Table S2. Diameters of the rings and inner depressions of multiring basins measured from LOLA topography and GRAIL Bouguer anomaly data.
Table S3. Ring diameters and centroids for circles fit to the rings of multiring basins.
Table S4. Lunar peak-ring basins.
Table S5. Lunar impact structures ≥200 km in diameter with only one topographic ring and no interior peak ring or central peak structure.
Table S6. Lunar depressions suggested by GRAIL data to be degraded basins.
Table S7. Features in basin catalogs not meeting criteria for inclusion in this study.
References (*42–65*)

Supplementary Text

The information in this supplement is intended to support the material presented in the main text and to detail the criteria and methods used for identifying basins. Explanatory terminology and expanded descriptions are included for features in the catalog that are not well known or have not been resolved prior to GRAIL, including maps of topography and Bouguer anomaly with rings identified. Supplementary tables illustrate the categories of basins revealed by topography and GRAIL Bouguer gravity anomaly. Also listed are features proposed in previous catalogs that lack the signature of impact basins and thus are not confirmed in this study.

1 Morphology and morphometry of impact basins

It has long been known that lunar impact craters show systematic size-dependent changes in both morphology and morphometry (*3, 42)*. Simple bowl-shaped craters with circular rim-crest outlines dominate the fresh-crater population at diameters less than about 10 km. With increasing diameter from ~10 to ~30 km, the circular outlines become cuspate, convex-outward rim-crest outlines, and arcuate slumps partly fill and modify the bowl-shaped crater floor to form transitional craters. With further increases in diameter above ~30 km, circular to cuspate rim-crest outlines become irregular; smooth walls or arcuate slumps become systematic, multiple wall terraces; the crater floor flattens and shoals; and central peaks are commonly present. Such structures are known as complex craters.

For craters larger than ~200 km, a ring of peaks rather than a central peak forms between the center of the crater and the base of the crater wall, concentric with the rim crest. This ring of peaks is the defining characteristic of a peak-ring basin (*1, 2*). There are, however, structures that are transitional between complex craters and peak-ring basins. The term protobasin refers to some small (< 170 km) peak-ring basins that still retain a central peak (*7*).

Some impact structures larger than ~550 km display an additional concentric ring and are termed three-ring or multiring basins. Additional candidate concentric rings (*4, 5, 43)* have been proposed for some basins. Moreover, in well-preserved basins, an inner depression has been identified.

Several studies have characterized the population of lunar craters (*6, 44)*. The comprehensive data sets of the Lunar Reconnaissance Orbiter (LRO) mission (notably those from the Lunar Reconnaissance Orbiter Camera, or LROC, and the Lunar Orbiter Laser Altimeter, or LOLA) have permitted global high-resolution characterization of crater morphology and morphometry. A critical process undetermined by these studies, however, is the mechanism for basin ring formation.

Numerical simulation of basin formation (*10, 24–27*) will be required to understand ring formation fully, but a global reassessment of the locations and diameters of basin rings is required to constrain such numerical models. In this paper we have re-analyzed previously identified peak-ring and multiring basins with LROC and LOLA data to assess their certainty of identification. Using GRAIL Bouguer anomaly data we have identified the region of crustal thinning beneath each basin and correlated the diameter of the central positive Bouguer anomaly with basin ring diameters identified from surface morphology.

A major difficulty in assessing the detailed structure of basins is the influence of crater degradation processes on their defining features. The majority of peak-ring and multiring basins date from the early Imbrian, Nectarian, and pre-Nectarian periods (*5, 45)* when the impact flux was much higher than at present. For features of such ages, superposed impact events have resulted in substantial degradation at all scales. A single impact crater can degrade nearby craters

(*46*), superposed large impacts can completely obscure parts of peak rings (*7*), and volcanism can flood basin interiors, obscuring peak rings, scarps, and interior depressions (*47, 48)*. For example, ejecta from the Orientale basin (Fig. S7) has blanketed much of the older Mendel-Rydberg basin (Fig. S8), and mare volcanism has substantially altered the Imbrium basin (Fig. S9) by covering much of the annular extent of the rings, almost completely burying the peak ring, and completely flooding the interior depression to a depth of several kilometers.

The GRAIL gravity data provide a three-dimensional perspective on impact crater and basin substructure, partially offsetting the degradation effects of superposed craters and volcanism. We first analyzed three basin data sets (*5, 28, 43*) compiled with earlier, pre-LRO data. We assessed the presence or absence of each proposed ring, noted any changes in diameter from those of the original studies, and searched for additional rings not previously documented. We then searched for additional degraded basins in the GRAIL Bouguer gravity anomaly field. Ring assignments (main ring, intermediate ring, and peak ring) were inferred for multiring basins on the basis of the correlation of surface morphology and Bouguer gravity anomaly signature.

The basins recognized collectively from GRAIL and LOLA data, along with their dimensions, are listed in Table 1. Table S1 documents structures with diameters <200 km investigated for the characteristics of basins and for size–frequency distributions. Tables S2 through S6 list 11 multiring basins, 16 peak-ring basins, 30 sizeable impact structures with only one topographic ring and no interior peak ring or central-peak structure but peak-ring-like gravity, and 16 sizeable depressions that lack confidently measureable rings but are suggested by GRAIL to be degraded basins with a substantial (>130 mGal) Bouguer anomaly contrast. In the last case, the original crater diameters are inferred from GRAIL data and scaling relationships. Finally we list in Table S7 features that have appeared in earlier basin catalogs but lack both a substantial morphometric expression (confidently measurable rings or closed topographic depression on the basis of LOLA data) and a central Bouguer anomaly high. These features do not meet the criteria for identification as an impact basin.

2 Maps of impact basins

The Bouguer gravity anomaly associated with lunar basins reveals subsurface density anomalies, likely primarily associated with variations in crustal thickness. The Bouguer anomaly was calculated for a uniform density of 2500 kg m^{-3}. Regional lateral variations in crustal density of ±10% may be present (*23*), but their long-wavelength nature does not affect the sharp contrast of Bouguer anomalies within impact basins. Bouguer anomaly patterns at the longest wavelengths are not likely to be related to impact structures but are instead associated with lateral variations in either crustal thickness or crustal or mantle density. To suppress these signals, spherical harmonic degrees 1–5 of the Bouguer anomaly were set to zero. For each basin, we determined the Bouguer anomaly contrast, i.e., the difference in Bouguer anomaly between the central high and the annulus of negative anomalies, as described in Methods, excluding overlapping regions where noted.

Maps illustrating the basin topography from LOLA and the Bouguer anomaly, contoured at 50 mGal intervals, are shown in Figs. S1 through S17. Multiple rings are plotted with centers at a common origin, neglecting the small offsets obtained when fitting individual rings. The Mercator or oblique stereographic (conformal) projections show the concentric small circles that describe basin rings as sets of circles (not precisely concentric) on the maps. Identified or suggested main rings are shown as solid lines, innermost rings or peak rings are shown as dashed lines, intermediate rings are shown as dot-dash lines, and inner depressions are shown as dotted lines.

3 Multiring basins

All basins cataloged previously (*5*, *28*, *43*) were re-assessed with LOLA gridded topography (128 pixel/degree or ~237 m/pixel) and LROC wide-angle camera visual image mosaics at 100 m/pixel. Topographic rings were identified on the basis of preservation of scarps and discernible peaks, and arcuate topographic highs bounding central lows. We generally used the criteria of Fassett et al. (*49*) for recognizing and mapping basin rings and assigning confidence levels for these assignments. Rings mapped as certain have a mappable topographic signature along at least 50% of the basin circumference. Rings mapped as probable may be less than 50% complete or are degraded to a degree that makes their mapping less than certain. Rings mapped as possible are those that are the most uncertain, either because the rings formed only incompletely or because the structures have suffered extensive post-formation degradation. To measure the diameter of an interior peak ring, which is typically segmented and discontinuous, the peaks must be sufficiently numerous and spatially organized to form a mappable ring structure. Our criteria differ slightly from those of Fassett et al. (*49*) in that ring-like arrangements of wrinkle ridges are generally not considered as a basin "ring." A possible exception has been made for Serenitatis (Fig. S7), for which the wrinkle ridges have been interpreted to broadly outline a 416-km-diameter buried "Linné" ring on the basis of Lunar Sounder Experiment (*50*) data, and a Serenitatis North (*51*) structure, for which the circular Bouguer anomaly contours suggest an earlier basin that is now obscured. A ring-like wrinkle ridge could indicate a buried topographic ring or inner depression (see below), but it could also result from lithospheric loading by mare basalts and stresses induced by variations in topography and crustal thickness.

Where possible, we visually fit circles to each ring by locating the highest topographic points that best defined the locations of the crest of peaks and arcuate segments that make up the ring. This procedure differs slightly from those of some earlier measurements (*42*) for which the inner edges of ring segments were used, but it should be more reliable for highly degraded structures. Our ring diameter measurements are therefore expected to be slightly larger than some earlier measurements. For inner depressions, which are not defined by a ring of peaks but rather a topographic step interior to the smallest ring, we used the inner edge of the topographic break for measurement. As in the Orientale basin, this topographic break likely corresponds to the outer edge of the interior impact melt sheet that subsided vertically by thermal contraction (*52*). In many basins, the inner depression has been completely obscured by mare flooding. However, in locations of thinner mare fill, topographic breaks in slope and arcuate wrinkle ridges are still present and are inferred to define the position of the underlying inner depression. Because of the irregularity of the inner depressions and later modification by mare emplacement, their mapped locations and measured diameters are considered only approximate. As inner depressions are inferred to result from thermal-induced subsidence, we do not consider them to be primary basin rings in this analysis.

Measured ring diameters and their confidence levels are listed in Table S2 for those basins proposed earlier (*5*, *43*) to contain three or more rings. All such basins possess prominent Bouguer anomaly contrasts, and all except for Coulomb-Sarton and Serenitatis have at least two certain rings. A third intermediate ring is present in many of the basins, but such a ring has been mapped with a range of confidence levels. Many basins also contain a probable inner depression. Three basins (Nectaris, Orientale, and Crisium, Figs. S4, S7, S10) are considered to be certain multiring basins. Four basins (Mendel-Rydberg, Imbrium, Humorum, and Hertzsprung, Figs. S8, S9, S11, S12) are considered to be probable multiring basins, but there is uncertainty in the measured third ring. The remaining four basins (Serenitatis, Humboldtianum, Coulomb-Sarton,

and Smythii, Figs. S1, S13, S14, S15) have the least certain evidence for a third ring. We discuss in the next section the Moscoviense impact structure, for which multiple rings arguably result from a double impact (*41*). Table S3 lists the centers and diameters of all mapped rings as a great-circle distance. Little morphologic evidence was found for the presence of additional rings outside of the main topographic rim crest of Orientale, Imbrium, Serenitatis, or Crisium (cf., Fig. 1a in Pike and Spudis (*43*)). Many features used previously to suggest the presence of these rings consist instead of local crater rims that sometimes appear as locally arcuate segments that if connected together could mimic a portion of a ring. With the LOLA topographic data, none of these outer rings met our ring identification criteria. Similarly, our criteria exclude several depressions surrounded by rim crests of other basins, e.g., the proposed Lomonosov-Fleming (*5*) and Kohlschutter-Leonov basins (*29*) that lack distinctive topographic or gravity features.

The assignment of basin rings in Table S2 to the main, intermediate, and peak rings is made on the basis of comparisons of mapped rings with Bouguer gravity anomaly patterns. As described in the main text, peak-ring basins have radial Bouguer anomaly profiles that are well correlated with surface morphology. A central positive Bouguer anomaly has a diameter that corresponds closely to the diameter of the interior peak ring. Outward from the central positive anomaly is an annulus of negative Bouguer gravity anomalies that reaches a minimum between the peak ring and rim crest and extends outward to the main topographic rim. When a third ring is present, e.g., the Outer Rook ring of Orientale (Fig. S7), it is intermediate between the main and peak rings and is located within the annular negative Bouguer anomaly.

By analogy with the correspondence shown in Fig. 4 and the long-known relation for peak-ring basins that the main topographic rim is approximately twice its peak-ring diameter, the diameter of the central Bouguer anomaly of a multiring basin guides our selection of which ring corresponds to the basin rim-crest diameter. When multiple rings are present, we chose the ring that was closest to twice the Bouguer anomaly diameter to represent the basin diameter. Unlike the assumption adopted by Pike and Spudis (*43*), the main ring in Table S2 is not always the most prominent topographic ring, plausibly a result of topographic degradation.

4 Peak-ring basins and other sizeable lunar impacts

Peak-ring basins and protobasins were re-assessed and measured with LOLA and LROC WAC data by Baker et al. (*7*). Listed in Table S4 are 16 basins that represent transitional forms between smaller complex craters and the larger multiring basins of Table S2. Each of these basins possesses a prominent central positive Bouguer gravity anomaly.

Impact features >200 km in diameter that possess only a single measureable rim crest and no interior peak ring or central peak structure, but that are comparable in size to the peak-ring basins, are listed in Table S5. These features, such as Orientale Southwest (Fig. S7), may have formed with a partial or full interior peak ring, but incomplete ring development or later degradation limited evidence for this interior structure. Thirty such basins are recognized on the basis of their topographic and Bouguer anomaly signatures. All possess well-defined central Bouguer anomalies.

One such basin is defined by the 640-km-diameter ring that lies outward of and offset from the 421-km-diameter, mare-filled Moscoviense peak-ring basin (Fig. S16). A highly degraded outer ring is centered 60 km to the northeast of the center of Moscoviense and encloses a negative Bouguer anomaly annulus, transitioning to positive in the northeast quadrant, where a concentric partial inner ring merges with the main ring of Moscoviense. The central positive Bouguer anomaly is enclosed by a circle about half the diameter of the outer ring and is offset to

the northeast, consistent with a double-impact origin (*41*). The Bouguer anomaly high of the smaller Moscoviense basin (Fig. S16) is much more circular and has a considerably greater anomaly contrast than that of any similar sized feature. Moreover, models of crustal thickness indicate a nearly vanishing thickness at the center (20, 23), suggesting an impact into a previously impact-thinned crust. By these measures we include in this table a separate, larger, and older Moscoviense-North basin.

5 Basins without measurable rings that are identifed by GRAIL Bouguer gravity anomaly

From the relationships between surface structures and Bouguer anomaly for peak-ring and multiring basins, we next identified degraded basins on the basis chiefly of their gravitational structure, and we attempted to estimate their dimensions. The Mutus-Vlacq (*5*) depression is one such structure, enclosing a substantial Bouguer anomaly high, but its dimensions are considerably smaller than originally described. Azimuthal averages of topography provide an estimate of the average distance from the center of the structure, where topography reaches a local maximum. For those basins that lack a discernible rim crest, azimuthal averages of near-circular Bouguer anomaly highs are used to assign principal diameters following 2-to-1 scaling.

As discussed in the main text, Fitzgerald-Jackson (Fig. S2) does not meet our criterion for having two morphologically measurable rings (despite an inner ring having been mapped earlier (*6*)) since most of the topographic high that defines its rim crest (especially in the northern, eastern, and southeastern portions) consists of overlapping impact craters. Fitzgerald-Jackson is nevertheless recognized by GRAIL as a basin, and its Bouguer anomaly high suggests a larger impact structure. TOPO-22 (Fig. S17), for which Clementine topography suggested a 314-km-diameter main ring (*28*), likewise did not meet our criteria for mappable rings. This basin, west of Debye crater, has a large central Bouguer anomaly high with a nearly circular boundary and thus is estimated to have once had a ~500-km-diameter main ring. The Bartels-Voskresenskiy candidate basin southeast of Lorentz (Fig. S5) possesses a bullseye gravity pattern that hints at a partially preserved rim crest along the southwestern edge. The Sinus Aestuum area and the region surrounding a small crater “Copernicus H” (Fig. S6) are flooded by mare material, but the circular planform of the Bouguer anomaly resolves an underlying basin for which the outer diameter may be inferred from the scaling relation. The proposed basins underlying Mare Vaporum and Sinus Medii similarly are listed with inferred diameters. The Mare Australe basin as originally described (*5*) has neither discernible relief nor Bouguer contrast indicative of a basin. Its northern portion, however, contains an open depression with a near-circular positive Bouguer anomaly signature that we illustrate in Fig. S18 and confirm in Table S6. Not all circular Bouguer anomaly highs can be unambiguously ascribed to basins, however, and we exclude those associated with neutral or elevated topographic expression. The slight depression at 60°N, 105°E, north of Compton and east of Bel’kovich craters likewise has a positive Bouguer anomaly, but its lack of a surrounding negative anomaly annulus and the presence of an elevated volcanic complex suggests a magmatic rather than impact origin.

Features that appear in the catalogs of Wilhelms (*5*) and Frey (*28*) that did not meet our criteria for topographic rings and cannot be resolved by GRAIL are listed in Table S7. Some of these proposed impact basins take the form of irregular topographic depressions that could be highly degraded basins. However, they lack central Bouguer anomaly signatures, and their indistinct or nonexistent morphometric expression precludes confident identification of ring diameters. The proposed long-wavelength Chaplygin-Mandelshtam or St. John-Telius (*55*)

structure that overlies the northern rim lacks a topographic rim or a sharply defined Bouguer anomaly signature, unlike the ancient South Pole-Aitken basin, and thus cannot be confirmed. The Procellarum region has been suggested to result from an ancient giant impact (e.g., *5*, *56*), but there is no evidence from this study supporting an impact origin. This finding is consistent with previous GRAIL results that delineate a magmatic-tectonic structure (*57*) interpreted previously as remnants of an impact basin rim. Lastly, some additional features were described in a recent study (*58*) that utilized gravity derived from the SELENE mission, bandpassed from spherical harmonic degree 18 to 70, which provided insufficient resolution to ascertain the full population of basins.

Supplemental Figures

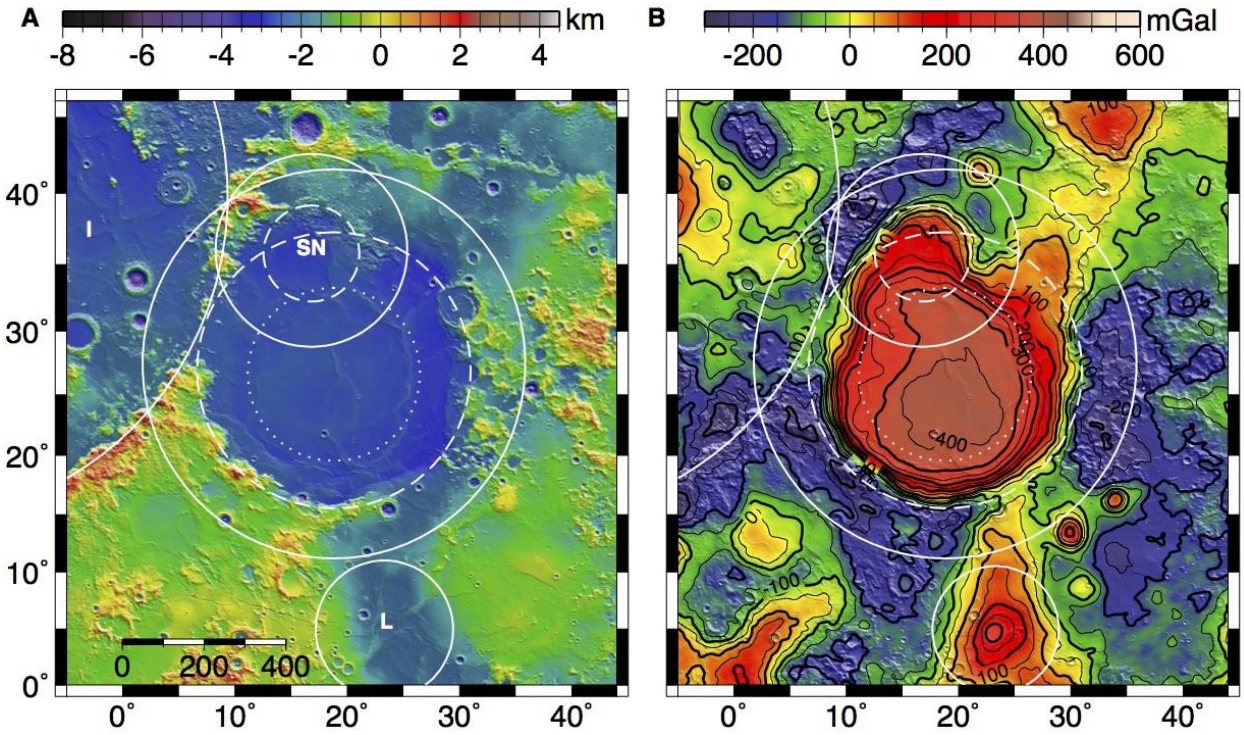

Figure S1. Serenitatis, Serenitatis North, and Lamont. (A) Topography of Serenitatis basin (*50*) in Mercator projection over shaded relief, interpreted as a multiring structure. The nearly concentric Vitruvius (~920 km diameter) and Haemus (~660 km diameter) rings, for which the topography is obscured by the later Imbrium (I) event, are shown by solid and dashed circles. The 420-km-diameter Linné ring (dotted) is mapped as a circular wrinkle-ridge feature conjectured to overly a peak ring. The Serenitatis North (SN) basin (*51*) and Lamont (L) basin are documented in Table S6. (B) The Bouguer anomaly (50-mGal contours) shows a 550-km-diameter mantle uplift and a second 210-km-diameter mantle uplift within the Serenitatis North basin that increases the apparent diameter of the gravity anomaly. The scale bar at the bottom in kilometers is approximate at the latitude shown, here and in subsequent figures.

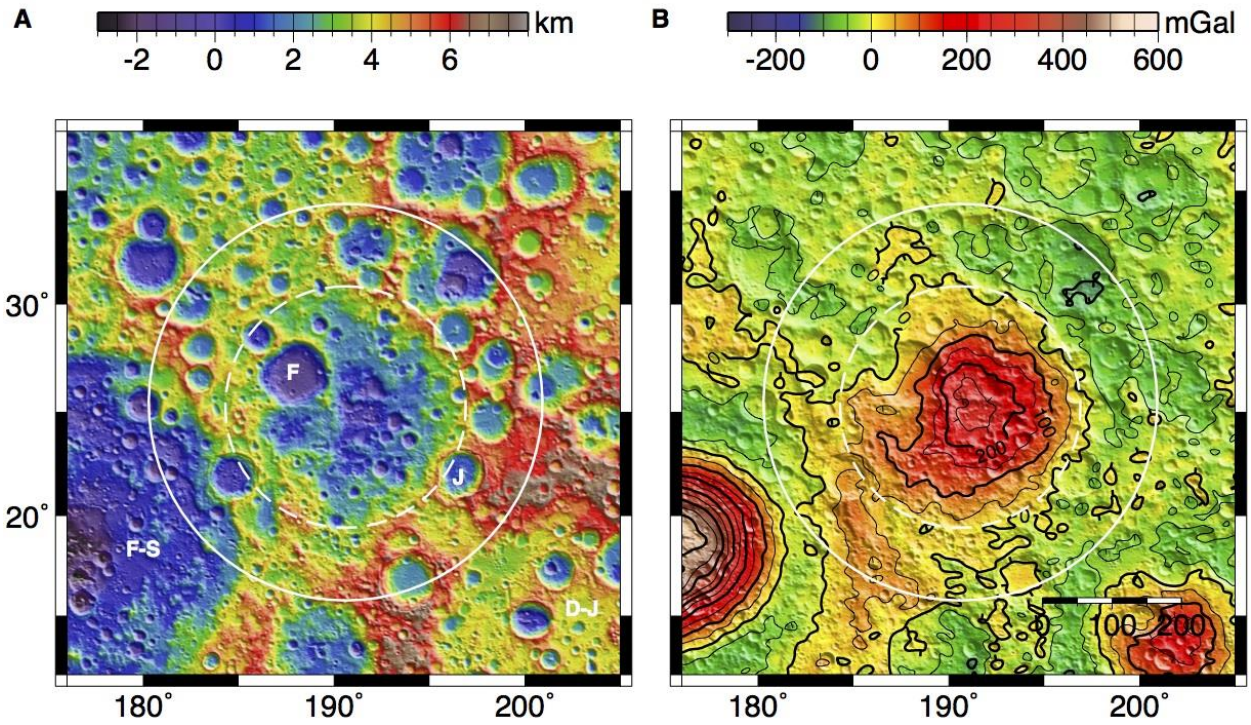

Figure S2. **Fitzgerald-Jackson.** (A) Basin topography showing a 346-km-diameter ring and possible outer ring (*6, 29*) in Mercator projection over shaded relief. Craters Fitzgerald (F), Jackson (J), and nearby basins Freundlich-Sharonov (F-S) and Dirichlet-Jackson (D-J) are labeled. (B) Bouguer anomaly (50-mGal contours) showing a near-circular central positive anomaly (dashed circle) with a disrupted northwestern boundary. The principal basin rim diameter and location have been estimated from the azimuthally averaged topography and gravity anomaly. In this and subsequent figure pairs, the assigned outer and interior rings are denoted by concentric solid and dashed circles, respectively.

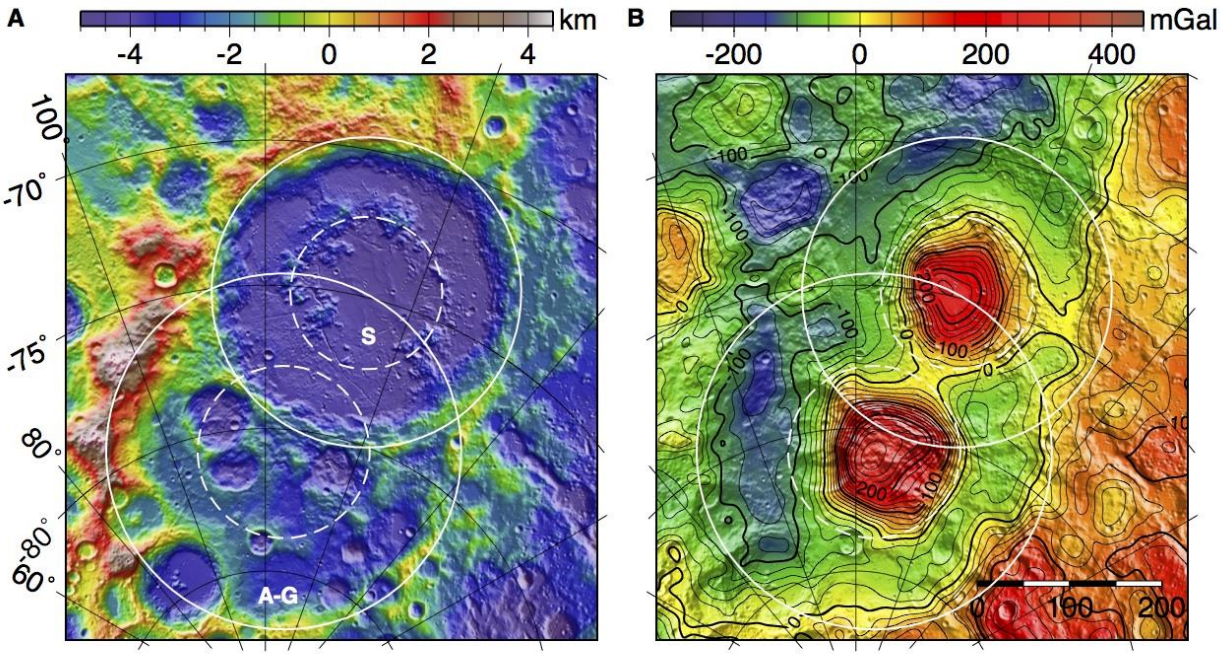

Figure S3. Amundsen-Ganswindt and Schrödinger. The 377-km-diameter Amundsen-Ganswindt (A-G) basin predates and lies southwest of the 326-km-diameter Schrödinger peak-ring basin (S) and is covered by its ejecta. (A) Topography in oblique stereographic projection. (B) Bouguer anomaly, 20-mGal contours, with inferred peak rings (dashes). A buried peak ring would coincide with the contours of the A-G gravity anomaly, but only a few remnants are mapped.

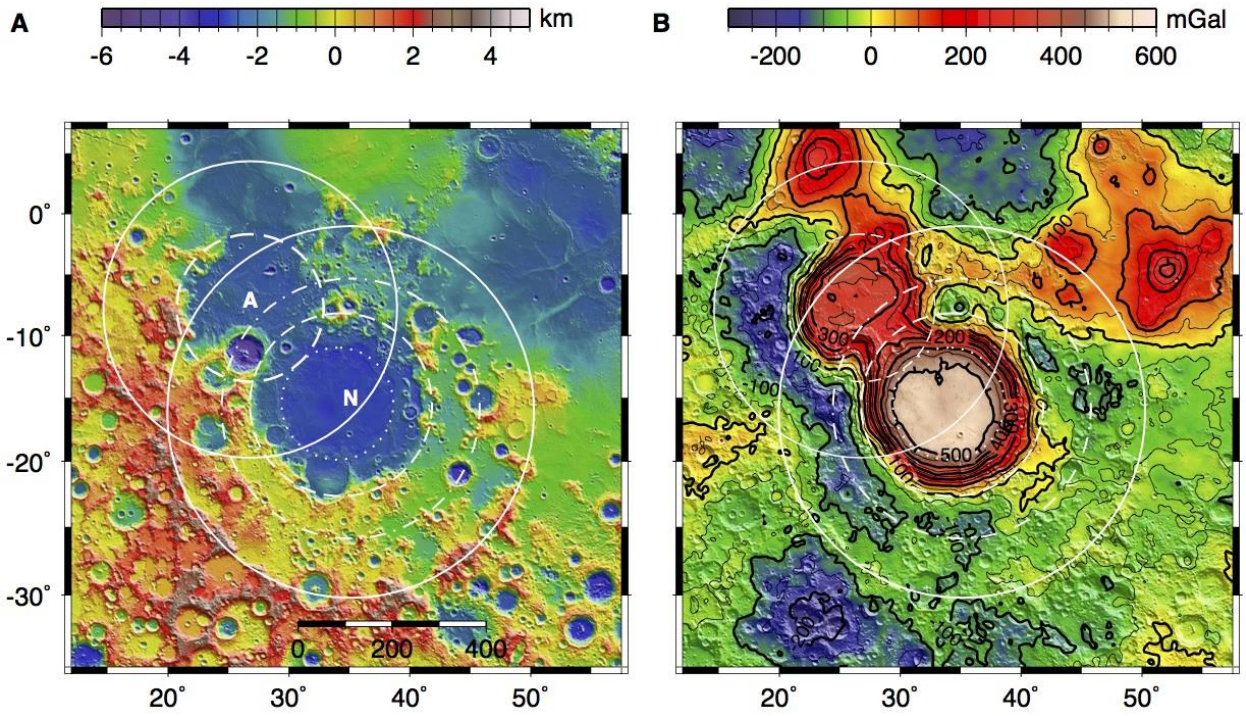

Figure S4. Nectaris and Asperitatis. The Nectaris multiring basin and the obscured Asperitatis (7.7°S, 26.8°E) basin are identified by letters N and A, respectively. (A) Topography over shaded relief in Mercator projection. Ring diameters and locations for Nectaris are shown as listed in Table S3: 885 km (solid), 440 km (dashes), and a 270-km-diameter inner depression (dots). An intermediate 623-km-diameter ring (dot-dash) bounds a portion of the southwestern terrace. Asperitatis has a probable preserved 365-km-diameter inner ring (dashes). (B) Bouguer anomaly over directionally shaded anomaly. The sharp, nearly circular boundary of the 330-mGal high over Asperitatis suggests an older, buried basin. From the negative Bouguer ring along the western edge and the scale of the inner ring we infer a 730-km-diameter outer ring (solid).

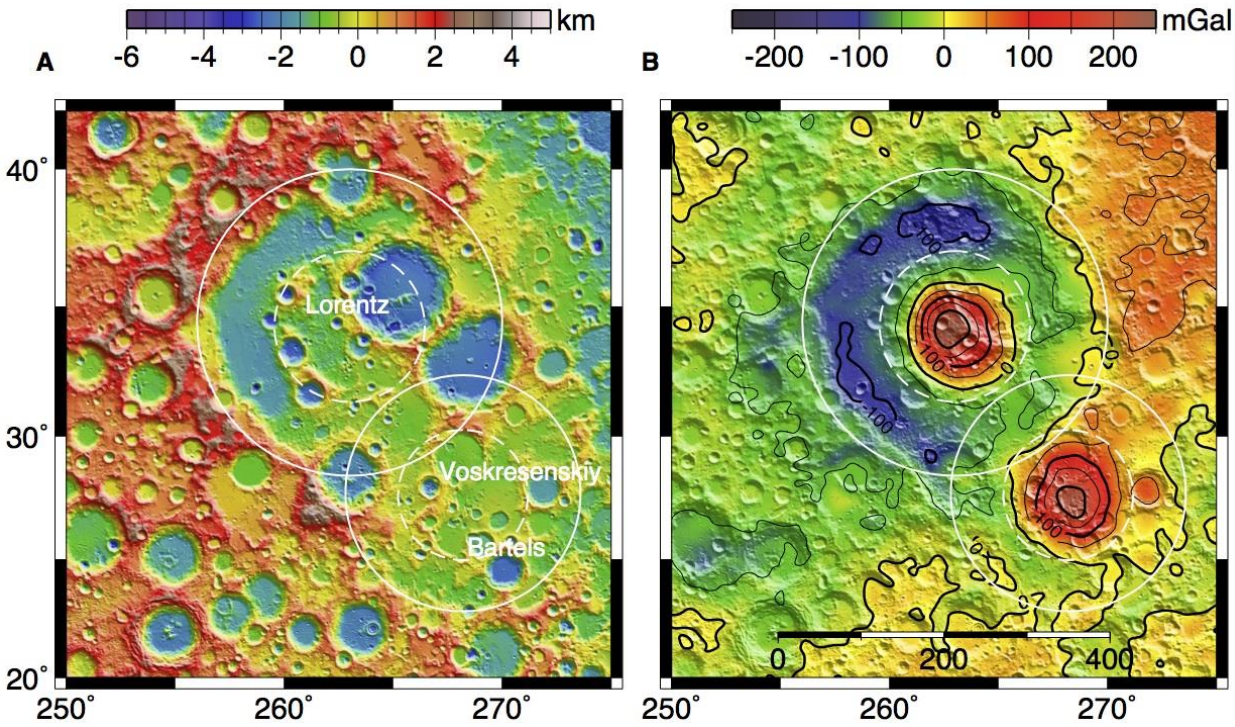

Figure S5. Lorentz and Bartels-Voskresenskiy. The Lorentz peak-ring basin overlaps a degraded impact crater named for two enclosed craters. (A) Circles denote the 351-km-diameter Lorentz basin with a 173-km-diameter peak ring (dashes) and the proposed 290-km-diameter basin at its southern boundary. The solid circle enclosing craters Bartels and Voskresenskiy suggests a rim crest that outlines a smoother region at -1 km elevation, which we interpret as the floor of a degraded basin. (B) Bouguer gravity anomaly shows two basins with positive anomalies. Dashed circles outline the peak ring of Lorentz and the 160-km-diameter inner ring of the proposed basin.

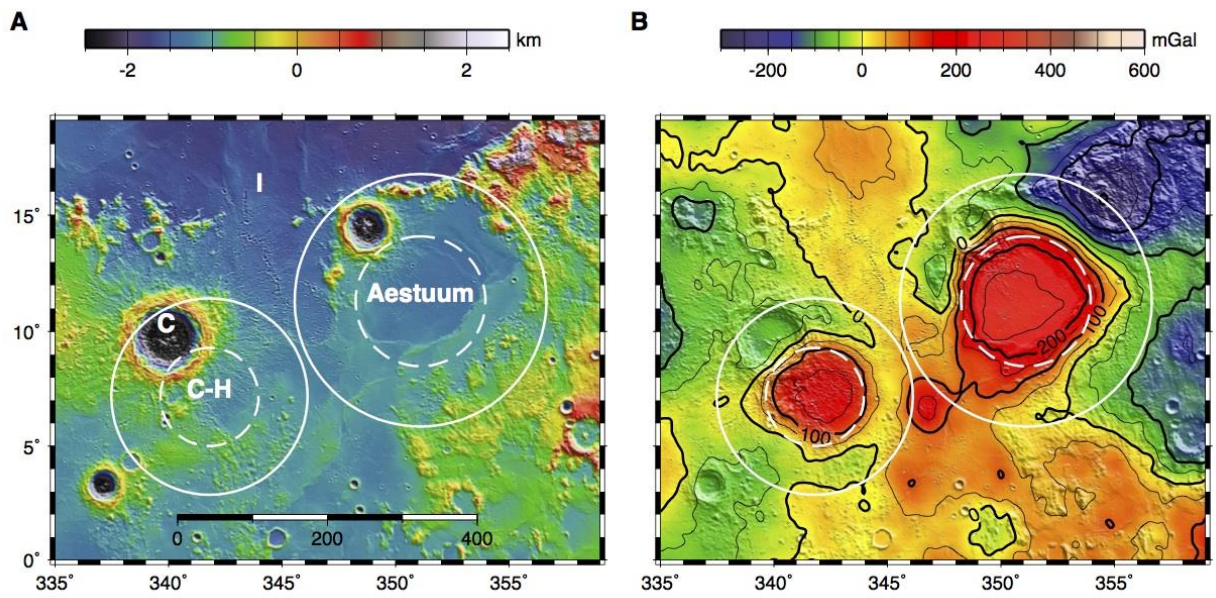

Figure S6. Copernicus-H and Aestuum. The proposed basins are named for a small dark-halo crater near the center of a 210-km-diameter topographic depression (C-H), and an indistinct 310-km-diameter feature (*28*) over the Sinus Aestuum area (left and right circles, respectively). (A) An impact origin for the indistinct topography of these two regions is corroborated by (B) central Bouguer gravity anomaly highs and annular lows, shown with the predicted outlines of obliterated rings. Extensive subsurface mare basalts are believed to underlie the region and may also contribute to the Bouguer anomaly highs. To the north is the nearly flooded outer ring of the Imbrium basin (I). The central peak of Copernicus (C) has olivine exposed as a major mafic mineral (*59*), and spinel-rich deposits are observed in Sinus Aestuum (*60*). The unusual exposures of mafic materials including spinel are observed in several regions of thinned crust (*61*), suggesting that these deposits may be related to uplift of mantle material (*62*) by an older impact.

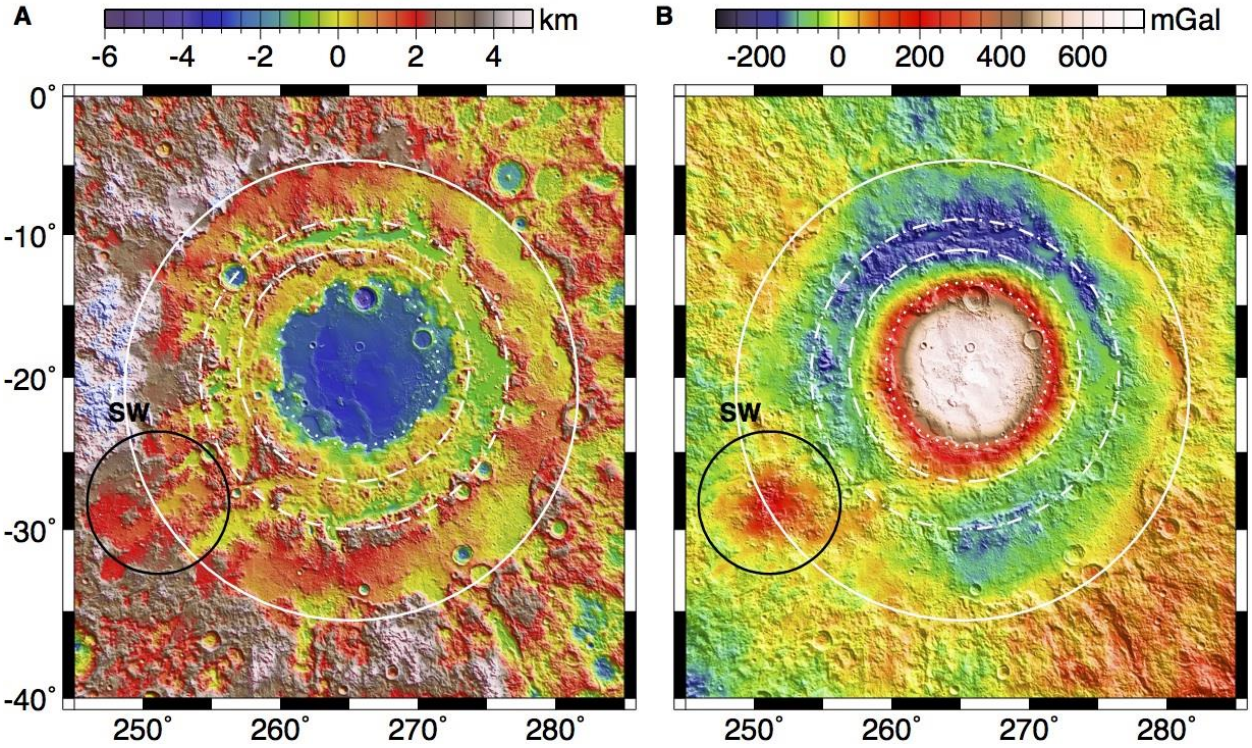

Figure S7. Orientale and Orientale Southwest. (A) Concentric topographic features and diameters for Orientale, the type example of a multiring basin, are as follows: main ring, 937 km; intermediate ring, 639 km (dot-dash); innermost ring, 481 km (dashed); inner depression, 341 km (dotted). The proposed 276-km-diameter "Orientale Southwest" basin (SW, black circle) is obscured by ejecta but was identified as a crater in LOLA topography (*6*). (B) A 735-mGal Bouguer anomaly high lies inside the inner Orientale ring, with a –100-mGal-average annular low situated on the intermediate ring (dot-dash). A 170-mGal high lies within the Orientale Southwest crater (dark circle).

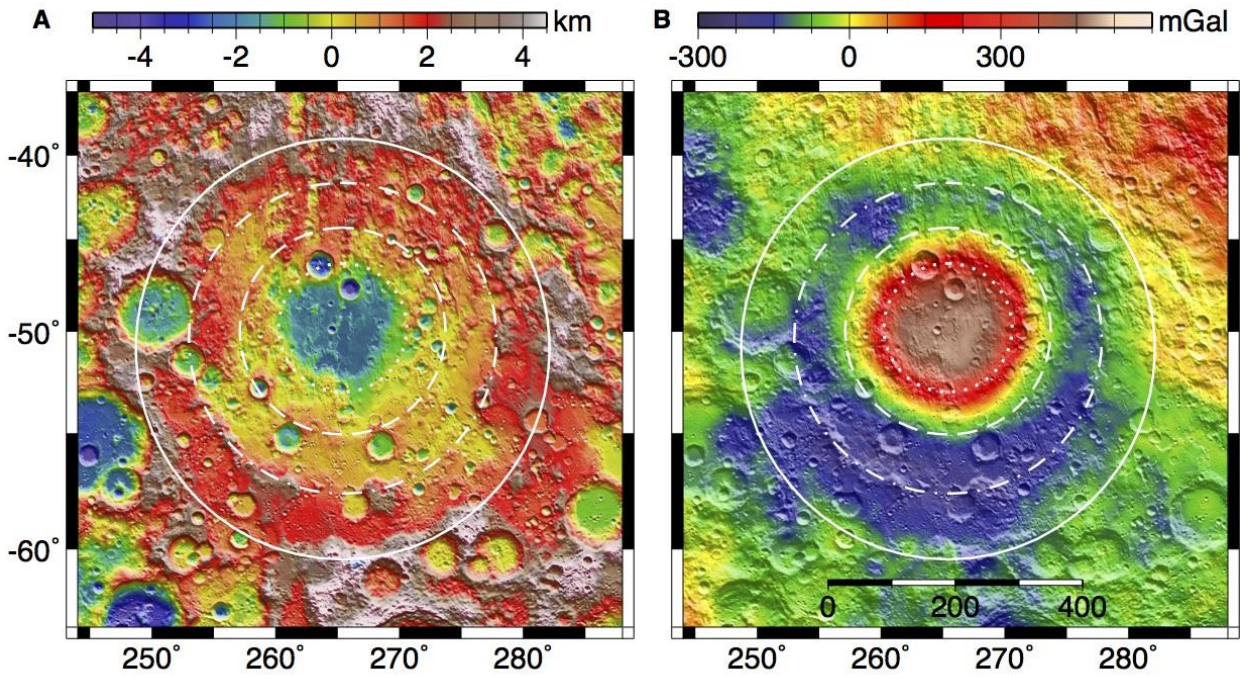

Figure S8. **Mendel-Rydberg.** (A) Outer ring and topographic rim crest of a multiring basin on the lunar limb, 650 km diameter (solid); intermediate ring, 485 km (dot-dash); probable inner peak ring, 325 km (dashed); and inner depression, 203 km (dotted). Ejecta from the Orientale basin to the north obscure the ring characteristics. (B) The central Bouguer anomaly high, with a 500-mGal anomaly, is enclosed by the 325-km-diameter inner ring.

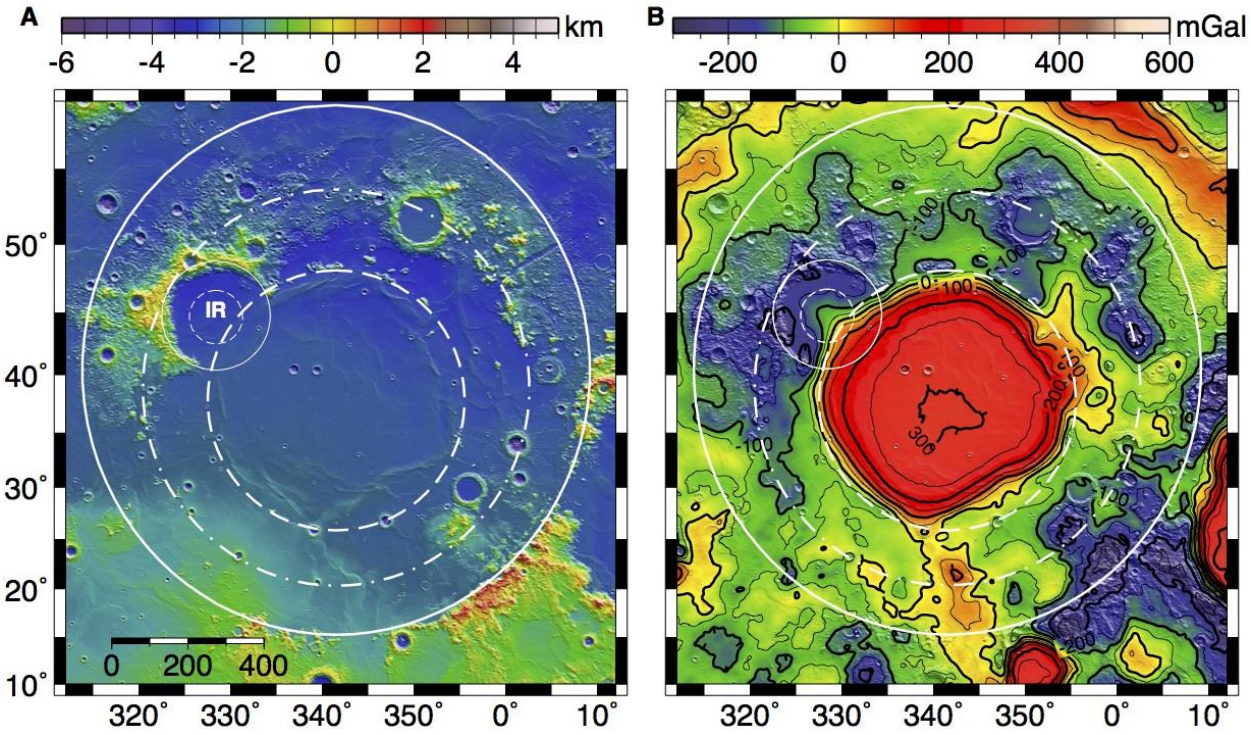

Figure S9. Imbrium and Iridum. (A) Topography shows nearly concentric main, probable intermediate, and inner rings as mapped in this study. IR denotes the 255-km-diameter Iridum impact basin outlined by the Montes Jura in the northwest. (B) Bouguer gravity anomaly. The Imbrium central anomaly is mainly confined within a circular pattern of wrinkle ridges and isolated peaks, interpreted as the inner ring. A smaller central Bouguer anomaly high centered within Iridum overlaps that of Imbrium.

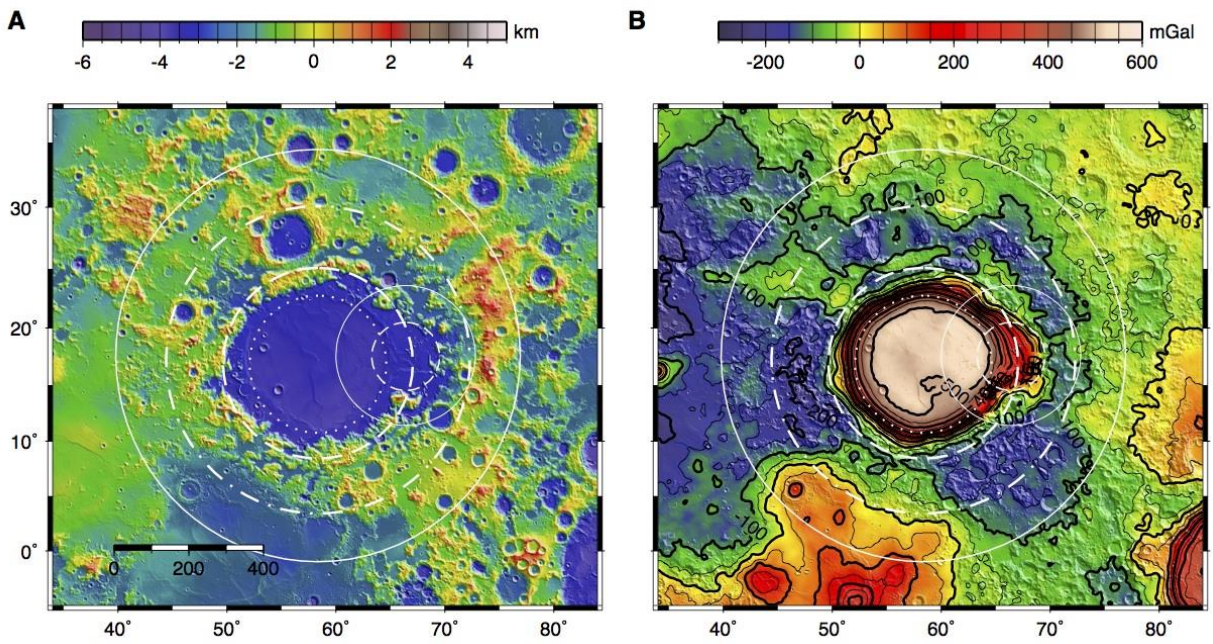

Figure S10. Crisium and Crisium East. (A) Topography with concentric rings for the Crisium basin: 1076-km-diameter outer ring; 809-km-diameter intermediate ring; 505-km-diameter inner ring; 364-km-diameter inner depression. The smaller concentric rings on the eastern edge are the proposed Crisium East or TOPO-05 (*28*) basin. (B) Bouguer gravity anomaly over shaded relief. The contours of the anomaly high enclose the inner ring of Crisium East, although a possible origin of this feature by an oblique Crisium impact has been suggested, e.g., by Wichman and Schultz (*63)* and Schultz and Stickle (*64)*.

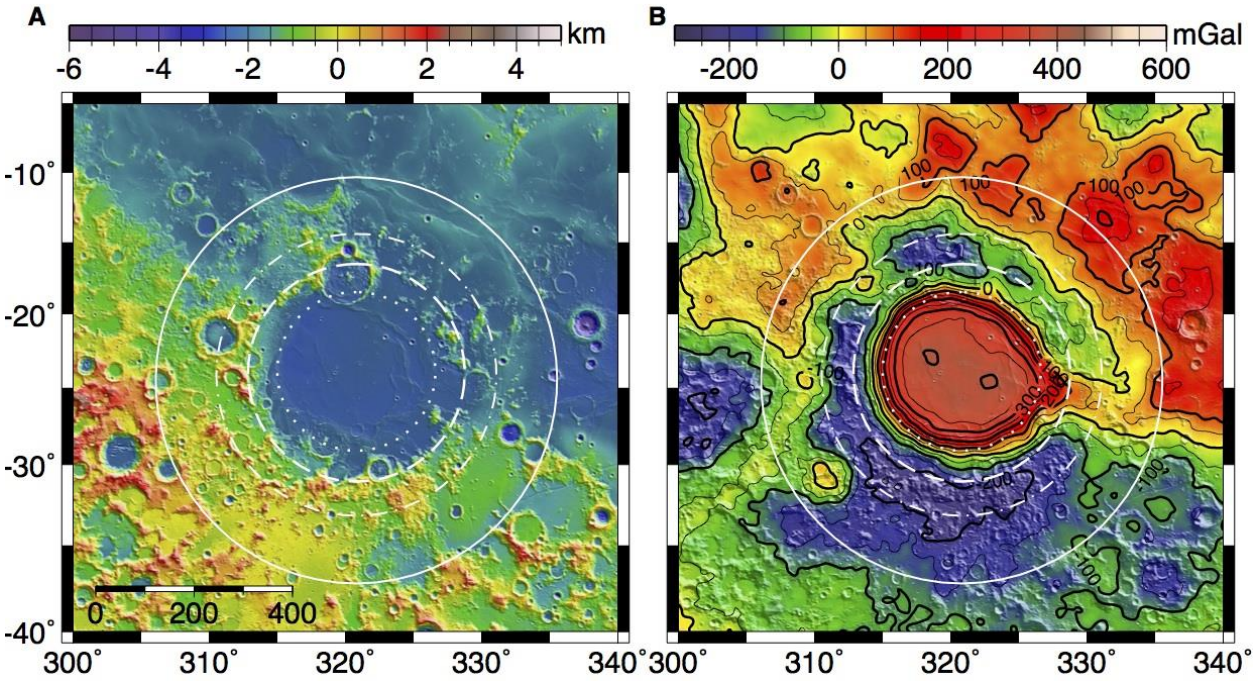

Figure S11. Humorum. (A) Topography shows the nearly concentric, 816-km-diameter main, 570-km-diameter intermediate, and 440-km-diameter inner rings of a probable multiring basin. (B) A Bouguer anomaly high is enclosed by a peak ring, and the partially exposed intermediate ring coincides with a negative Bouguer anomaly annulus.

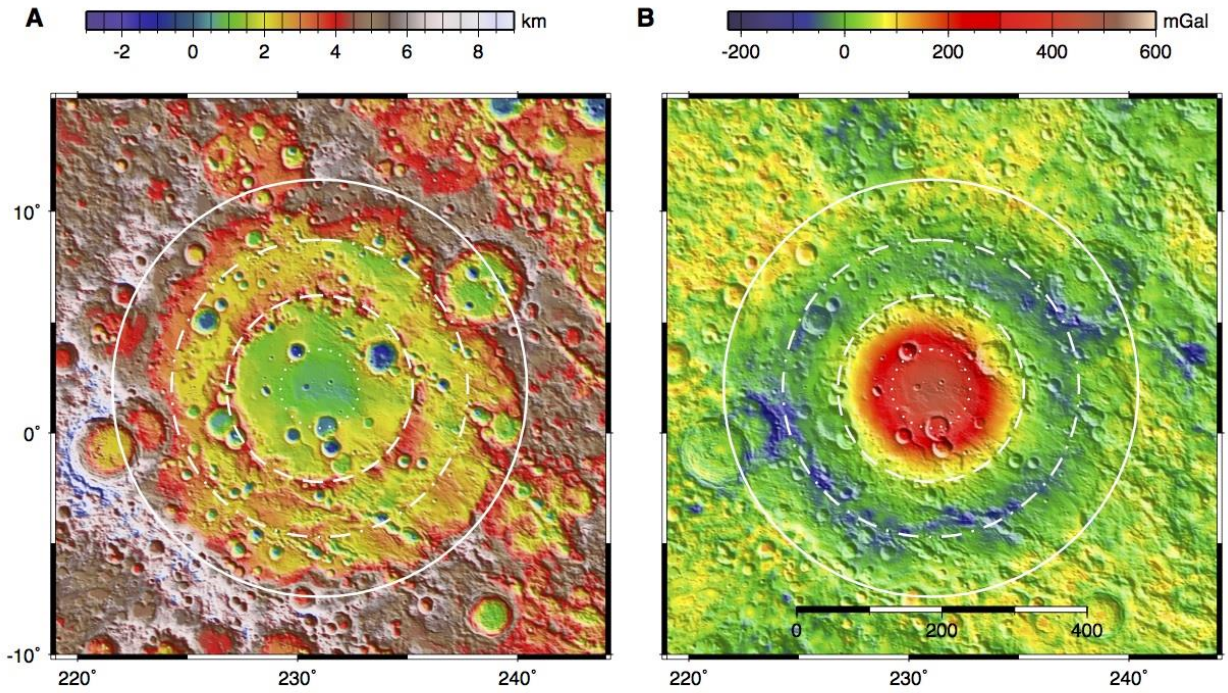

Figure S12. Hertzsprung. (A) Topography shows the 570-km-diameter main ring, the 408-km-diameter intermediate ring (expressed as a topographic step), and the 255-km-diameter inner ring of a probable multiring basin, with a 108-km-diameter inner depression (dotted circle). (B) The Bouguer anomaly high is enclosed by the inner peak ring.

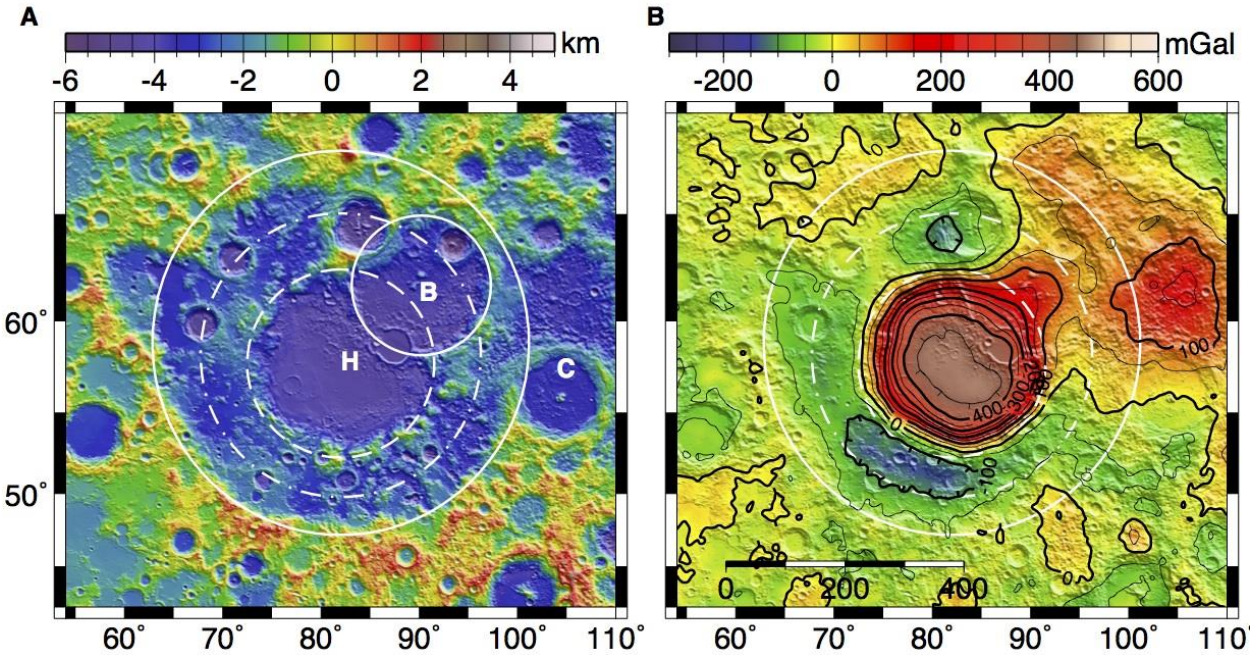

Figure S13. Humboldtianum and Bel'kovich. (A) Topography of Humboldtianum (H) shows

nearly concentric, 618-km-diameter main, possible 463-km-diameter intermediate, and 310-km-diameter inner rings, except where the Bel'kovich basin (B) and Compton (C) craters are superposed. (B) The Bouguer anomaly high is enclosed by the inner ring, and the main ring encloses a negative anomaly annulus except where Bel'kovich interferes. A large volcanic complex north of Compton produces a Bouguer anomaly high without a surrounding negative annulus and is not considered a basin in this study.

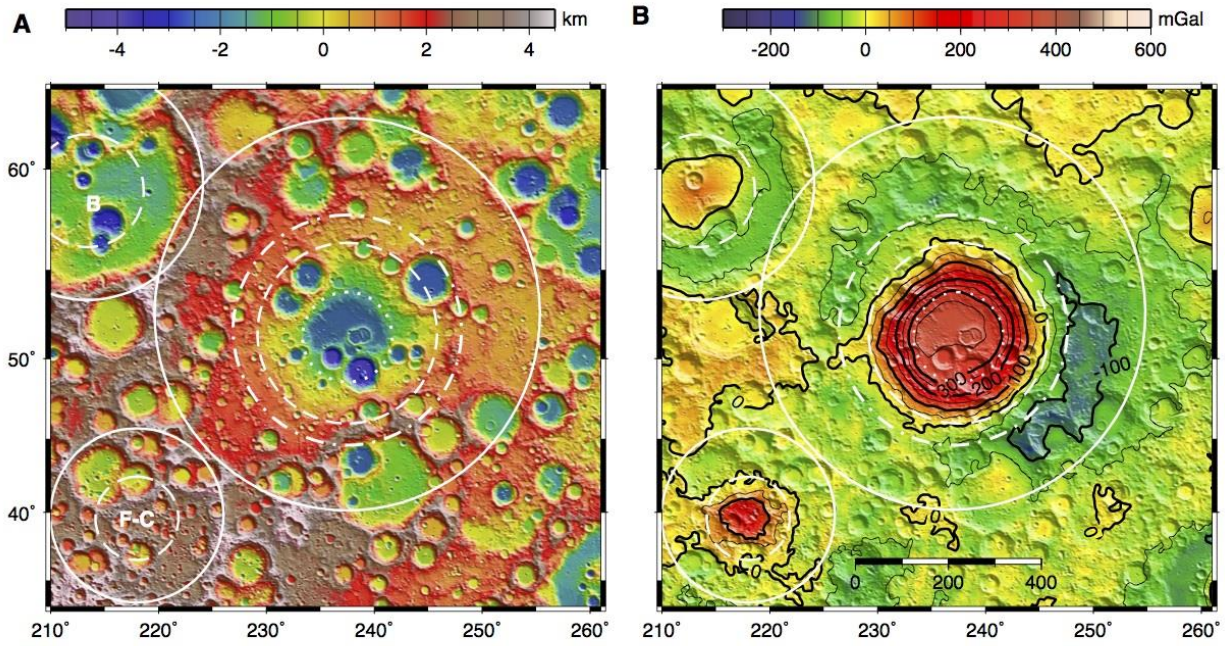

Figure S14. Coulomb-Sarton and Fowler-Charlier. (A) Topography shows Coulomb-Sarton (*2, 5*) (51.2°N, 237.5°E), a possible multiring basin with a 672-km-diameter outer rim crest (solid) and a 315-km-diameter inner topographic ring (dashed) that had previously been catalogued as the main ring (*6*) but is identified here as the innermost ring. A break in the topography (400 km diameter, dot-dash) represents a possible intermediate ring. An inner depression (158 km diameter, dotted) is shown. The Birkhoff peak-ring basin (B) is at the upper left, and the proposed 374-km-diameter Fowler-Charlier (*29*) basin (F-C) is at the lower left. (B) The Bouguer anomaly high is enclosed by the innermost ring. The rim crest and intermediate topographic rings enclose the annular Bouguer anomaly low.

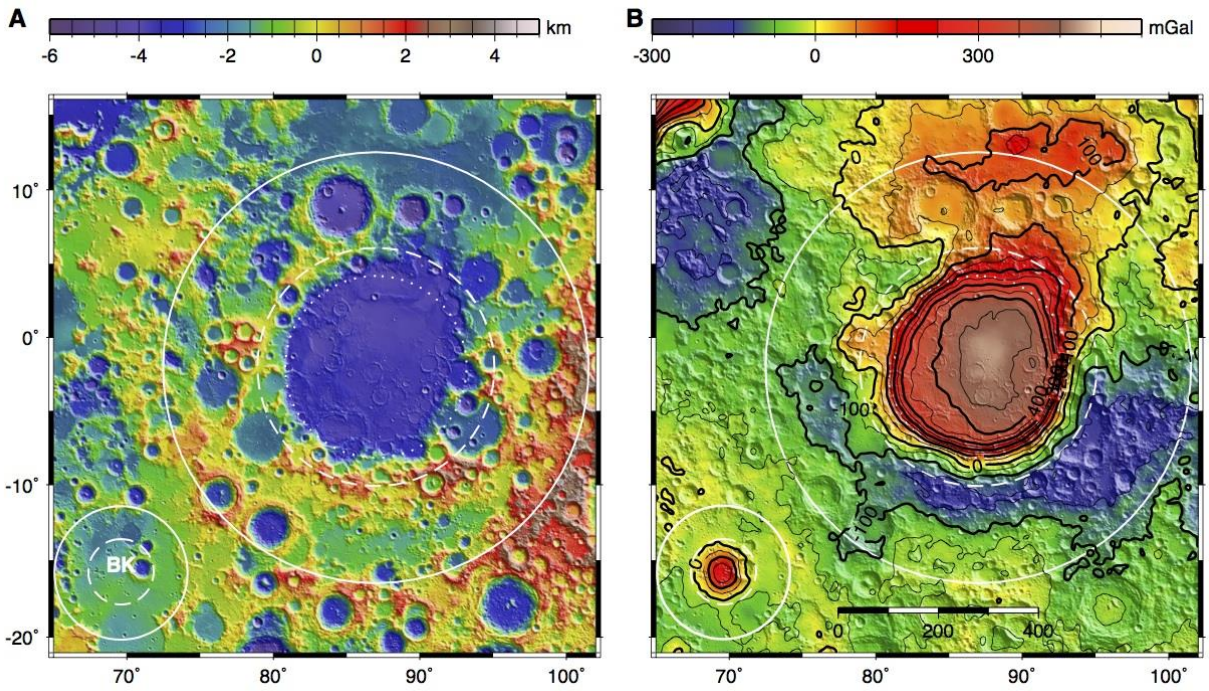

Figure S15. Smythii and Balmer-Kapteyn. (A) Topography shows a possible multiring basin with a 880-km-diameter rim crest, a 480-km-diameter peak ring, and a 375-km-diameter inner depression. A proposed 740-km-diameter intermediate ring (*5*) is not resolved. BK denotes the proposed Balmer-Kapteyn (*29*) basin and possible obscured peak ring. (B) Bouguer gravity anomaly shows a near-circular anomaly high and partial negative anomaly annulus within each basin.

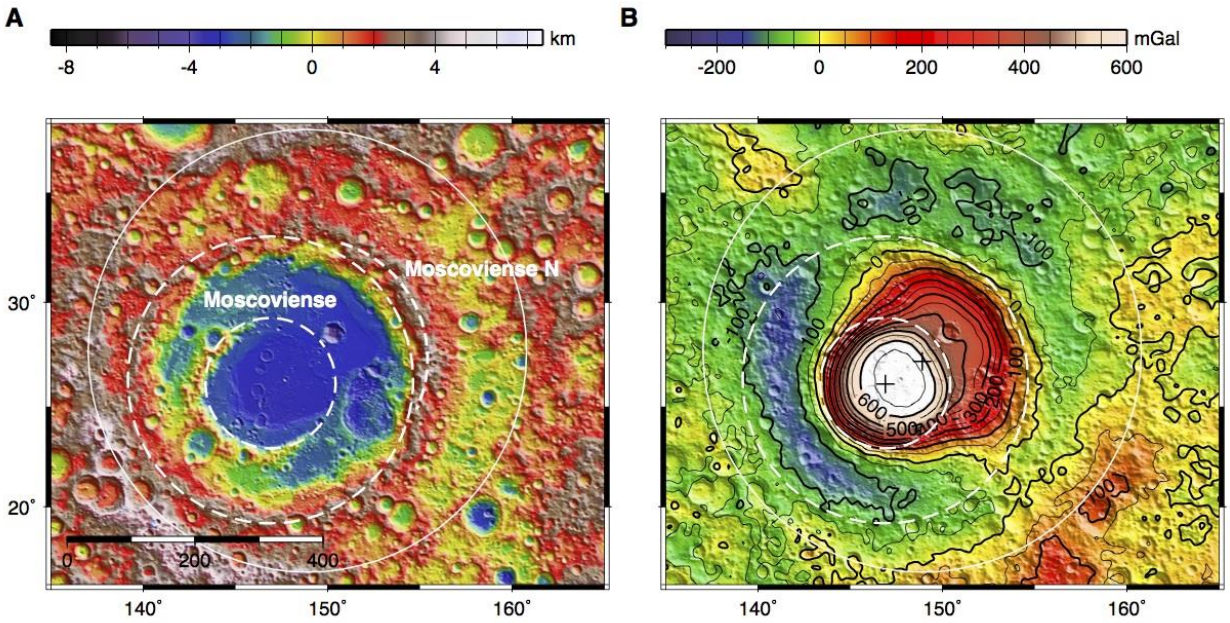

Figure S16. **Moscoviense and Moscoviense North**. (A) Topography shows a 421-km-diameter outer ring (Moscoviense) nearly concentric with a 192-km-diameter peak ring (dashed). These rings are offset from a 640-km-diameter ring (solid). Following Ishihara et al. (*41*) we interpret the two smaller concentric rings as the peak ring and main ring of an impact basin that formed within an earlier "pre-Moscoviense" basin, of which the main ring and a quarter arc of a peak ring (dashed) are preserved. We designate the earlier basin as Moscoviense North. (B) The central positive Bouguer anomaly exhibits two components: a ~350-mGal plateau with a surrounding ~100 mGal anomaly low enclosed by the Moscoviense North basin ring, and an inner component reaching a maximum of 680 mGal coincident with the smaller peak ring. The centers of the Moscoviense basin rings and of the outermost Moscoviense North ring are shown by plus symbols, offset by ~80 km.

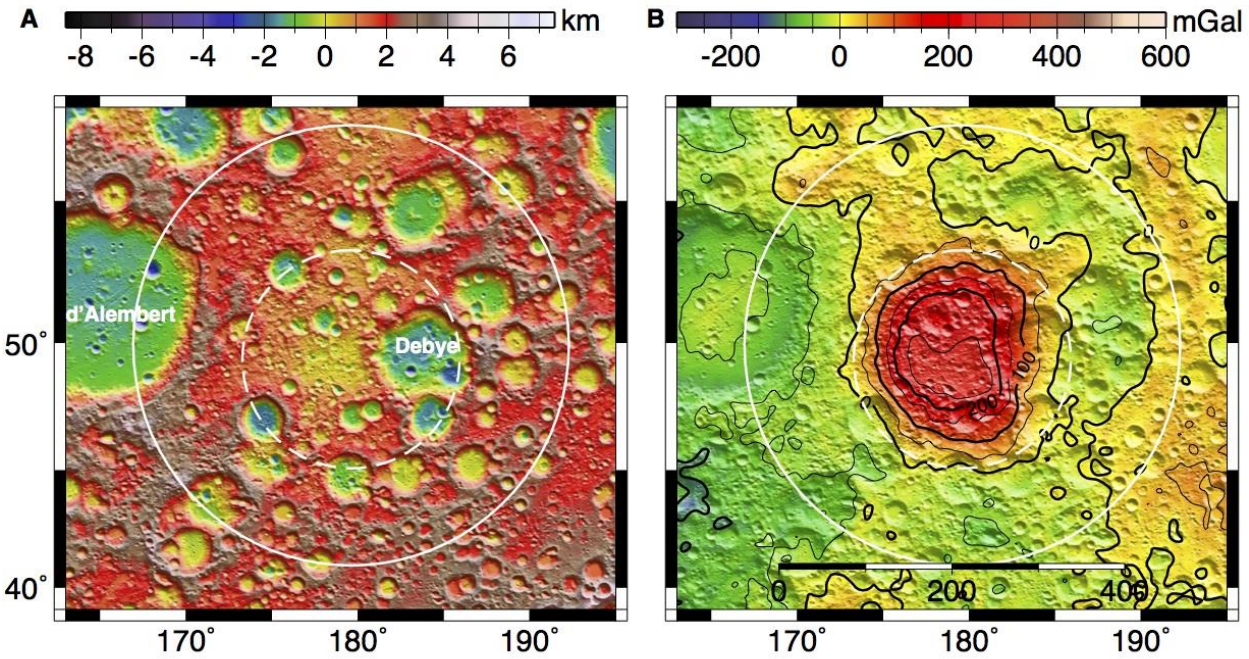

Figure S17. TOPO-22. (A) Topography of this proposed basin (*28*) shows an indistinct, ~500-km-diameter topographic crest (solid circle) surrounding a depression (49.4°N, 179°E) with an uncertain, 250-km-diameter ring (dashed circle) disrupted by the younger peak-ring basin d'Alembert to the west. (B) The Bouguer anomaly map shows a ~250-mGal central high and surrounding low corresponding to the proposed basin. Crater Debye (49.6°N, 184°E) disrupts the otherwise circular outline of the central region of thinned crust.

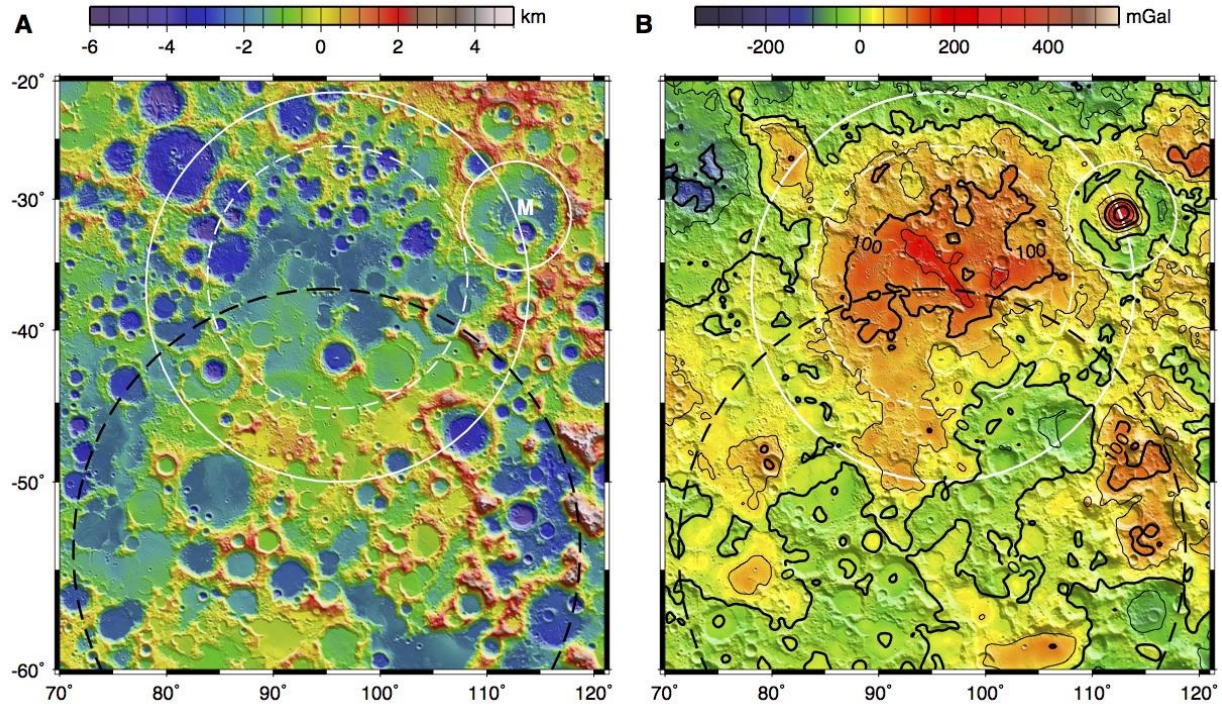

Figure S18. Australe North. (A) Topography of the proposed Mare Australe basin (*5*) enclosed by the black circle exhibits positive relief, casting doubt on an impact origin. However, the mare corresponds in part to a 600-km-diameter depression (dashed white circle) for which the topography suggests a large partially preserved basin (solid circle) adjoining the peak-ring basin Milne (M). (B) The Bouguer anomaly map shows a muted circular positive anomaly, flanked by lesser positive anomalies enclosed by a relatively negative annulus.

Table S1. Lunar craters < 200 km in diameter suggested from LOLA data. Additional craters >160 km in diameter were assessed for this study, chiefly from Head et al. (*6*). Names are approved by the International Astronomical Union, except where denoted by an asterisk (*) (*5*, *29*, *64*) or (**), the latter symbol indicating names assigned here on the basis of a nearby feature. Descriptions: CP = central peak; protobasin refers to small peak-ring basins that retain a central peak.

Name	Latitude (°N)	Longitude (°E)	Rim crest diameter (km)	Notes and additional ring diameters	Bouguer anomaly contrast (mGal)
Maginus	-50	353.7	160		3 ± 4
Rowland	56.9	197.33	160		3 ± 9
Cockroft-Evershead*	36.6	196.15	160		16 ± 14
Keeler	-9.70	161.9	161	CP	9 ± 6
Riccioli	-2.8	285.5	161	Floor-fractured	65 ± 19
Herschel	62.3	318.14	163		-48 ± 8
Riemann	38.9	86.8	163		-3 ± 5
Richardson	31.2	100.1	163		45 ± 10
Ptolemaeus	-9.3	358.1	164		7 ± 15
Drygalski	-79.8	272.1	165		-43 ± 2
Compton	55.92	103.96	166	Protobasin, 73-km-diameter inner ring	-12 ± 6
Schrödinger-Zeeman*	-80.8	191	166	Proposed 250-km-diameter ring (*29*) not confirmed	23 ± 16
Hecataeus	-21.8	79.4	167		-28 ± 2
Lippman	-55.44	245.8	168		-4 ± 18
Heaviside	-10.34	166.84	168		-4 ± 7
Roszhdestvensky	85.166	200.5	169		-7 ± 4
Sommerfeld	65.2	197.6	169		-7 ± 8
Joliot	25.86	93.44	169		19 ± 4
Hausen	-65.34	271.24	170	Protobasin, 55-km-diameter inner ring	1 ± 10
Vertregt	-19.16	171.16	171		33 ± 27
Struve	23.59	283.25	171		9 ± 17
Von Kármán M	-44.6	176.0	172		11 ± 10

Name	Latitude (°N)	Longitude (°E)	Rim crest diameter (km)	Notes and additional ring diameters	Bouguer anomaly contrast (mGal)
Hilbert	-17.9	108.2	173	CP	5 ± 4
Chebyshev	-34	227	175		30 ± 11
Fabry	43.0	100.8	177	CP	3 ± 6
Wugang*	13	189.5	177	Proposed by Chang'e-1 team (*65*)	1 ± 13
Petavius	60.6	-25.4	180	CP	29 ± 7
Kostinskiy	14.7	119.8	181		23 ± 7
Baldet-Minkowski*	-53.5	209.75	182		42 ± 9
Mandel'shtam	5.6	162.3	184		-18 ± 4
Tsiolkovsky	-20.2	129.0	185	CP	-2 ± 9
Einstein	16.76	271.42	185		-1 ± 4
Becvar	-2.75	124.9	187		3 ± 4
Zeeman	-75.0	224.4	190		41 ± 28
Galvani-Bunsen*	46.6	275.4	193		1 ± 14
Cognitum**	-9.3	335.5	197	Mare feature	84 ± 14
Janssen	-45.2	40.8	199	Floor-fractured	7 ± 7

Table S2. Diameters of the rings and inner depressions of multiring basins measured from LOLA topography and GRAIL Bouguer anomaly data. Multiring basins in this list were proposed by Wilhelms (*5*) and Pike and Spudis (*43*) and reanalyzed here. Following Pike and Spudis (*43*) and Fassett et al. (*45*), the confidence in the ring observations is given by { }= suggested by scaling, [ ] = possible, ( ) = probable, all others = certain. Multiring certainty is determined by the measured rings and their associated levels of confidence and diameters. A "multiring basin," which is classically defined as a basin with three or more concentric rings (*1*), is considered certain for basins with strong confidence in ring observations totaling at least three in number. Probable basins are likely to be multiring basins, but the poor preservation or development of a third ring structure precludes a confident ring measurement for these rings. Possible basins have rings that are either highly uncertain or missing, due to lack of preservation or lack of formation. Of the possible multiring basins, Humboldtianum and Smythii have two certain rings, whereas Coulomb-Sarton and Serenitatis have poorly preserved topographic rings but topography suggestive of multiple rings. Imbrium rings are only partially preserved, and different rings have been identified by previous workers (*5, 43*).

Name	Main ring diameter (km)	Intermediate ring diameter (km)	Inner ring diameter (km)	Inner depression diameter (km)	Multiring certainty
Hertzsprung	571	(408)	256	(108)	probable
Humboldtianum	618	[463]	322	[197]	possible
Mendel-Rydberg	650	485	(325)	203	certain
Coulomb-Sarton	[672]	(401)	(315)	158	possible
Humorum	816	(569)	441	(322)	probable
Smythii	878		484	(375)	possible
Nectaris	885	623	440	(270)	certain
Serenitatis	[923]	660	{416}	[316]	possible
Orientale	937	639	481	341	certain
Crisium	1076	(809)	505	(364)	probable
Imbrium	1321	(1012)	676	--	probable

Table S3. Ring diameters and centroids for circles fit to the rings of multiring basins.

	Main ring			Intermediate ring			Inner ring			Inner depression		
Name	Diam-eter (km)	Latitude (°N)	Longitude (°E)	Diam-eter (km)	Latitude (°N)	Longitude (°E)	Diam-eter (km)	Latitude (°N)	Longitude (°E)	Diam-eter (km)	Latitude (°N)	Longitude (°E)
Hertzsprung	571	1.92	230.94	408	2.22	231.13	256	2.00	231.22	108	2.04	231.22
Humboldt-ianum	618	57.27	82.01	463	57.30	83.00	322	57.75	82.84	197	57.80	82.71
Mendel-Rydberg	650	-49.53	266.08	485	-49.67	265.56	325	-49.69	265.47	203	-49.91	265.67
Coulomb-Sarton	672	51.26	236.93	401	51.20	236.99	315	51.24	237.48	158	51.16	237.41
Humorum	816	-23.69	320.86	569	-23.89	320.74	441	-24.28	320.62	322	-23.92	320.67
Smythii	878	-2.51	86.92	484	-1.92	87.25	--	--	--	375	-1.71	87.36
Nectaris	885	-15.61	35.13	623	-15.39	34.39	440	-15.44	34.33	270	-15.43	34.01
Serenitatis	923	26.46	19.24	661	26.48	18.85	416	25.19	18.81	--	--	--
Orientale	937	-20.10	265.14	639	-19.44	265.32	481	-19.01	265.31	341	-19.01	265.54
Crisium	1076	17.27	59.64	809	17.29	59.79	505	16.81	58.41	364	16.92	58.50
Imbrium	1321	36.51	341.85	1012	37.87	340.74	676	37.26	341.34	--	--	--

Table S4. Lunar peak-ring basins. The list of basins follows Baker et al. (*7*). Names are approved by the International Astronomical Union, except where denoted by an asterisk (*) (*5*).

Name	Latitude (°N)	Longitude (°E)	Main ring diameter (km)	Peak ring diameter (km)	Bouguer anomaly diameter (km)	Bouguer anomaly contrast (mGal)
Schwarzschild	70.3	121.0	207	71	90 ± 27	40 ± 9
d'Alembert	51.05	164.8	232	106	128 ± 31	46 ± 6
Milne	-31.25	112.8	264	114	126 ± 14	195 ± 22
Bailly	-67.1	291.1	299	130	112 ± 18	94 ± 16
Poincaré	-57.3	163.1	312	175	188 ±23	185 ± 11
Planck	-57.4	135.1	321	160	138 ±10	167 ± 52
Schrödinger	-74.9	133.5	326	150	152 ± 24	240 ± 19
Mendeleev	5.5	141.1	331	144	156 ± 25	159 ± 33
Birkhoff	58.9	213.4	334	163	126 ±17	90 ± 16
Lorentz	34.3	263.0	351	173	156 ± 13	240 ± 38
Schiller-Zucchius*	-55.7	314.8	361	179	210 ± 23	331 ± 15
Korolev	-4.44	202.53	417	206	204 ± 31	173 ± 15
Moscoviense	26.1	146.9	421	192	210†	632 ± 27
Grimaldi	-5.1	291.3	460	234	220 ± 20	431 ± 15
Apollo	-36.1	208.3	492	247	262 ± 18	329 ± 10
Freundlich-Sharonov*	18.35	175.2	582	318	318 ± 18	528 ± 18

† Diameter estimated excluding the portion ascribed to the Moscoviense North basin.

Table S5. Lunar impact structures >200 km in diameter with only one topographic ring and no interior peak ring or central peak structure. Names given are IAU approved names except when followed by an asterisk (*). Names with asterisks are from previous catalogs (*5*, *29*). Names with two asterisks (**) are provisional names based on nearby features. Latitude, longitude, and diameters are re-estimated from the tables indicated in the following references: (*54*), Table 2; (*53*) semimajor/semiminor axes for outer ellipse of South Pole-Aitken basin; (43) Table 2; (*28*), Table 1; (*6*), online crater database.

Name	Latitude (°N)	Longitude (°E)	Main ring diameter (km)	Morphology	Reference	Bouguer anomaly contrast (mGal)
Schickard	-44.5	305.0	206	1 ring	(6)	59± 9
Wegener-Winlock*	40.2	251.6	206	1 ring	(6)	36 ± 7
Humboldt	-27.1	81.0	206	Ringed peak cluster	(6)	52 ± 14
Oppenheimer	-35.4	194.0	206	1 ring	(6)	59 ± 9
Galois	-14.1	207.7	210	1 ring	(6)	6 ± 14
Rupes Recta**	-22.5	353.0	212	1 ring	(6)	25 ± 14
Keeler West**	-10.1	156.8	219	1 ring	(6)	3 ± 20
Deslandres	-32.6	354.7	220	1 ring	(6)	142 ± 19
Clavius	-58.8	346.0	220	1 ring	(6)	8 ± 9
Poczobutt	57.7	260.4	225	1 ring	(6)	77 ± 12
Pasteur	-11.5	104.8	231	1 ring	(6)	45 ± 9
Landau	42.2	240.8	236	1 ring	(6)	66 ± 9
Campbell	45.5	153.0	237	1 ring	(6)	43 ± 10
Fermi	-19.8	123.4	241	1 ring	(6)	79 ± 6
Von Kármán M	-47.1	176.2	245	1 ring	(6)	148 ± 16
Leibnitz	-38.2	179.2	247	1 ring	(6)	69 ± 18
Iridum**	44.8	328.3	252	1 ring	(6)	38 ± 14
Gagarin	-19.7	149.4	256	1 ring	(6)	44 ± 14
Balmer-Kapteyn*	-15.8	69.6	265	1 ring	(6)	192 ± 22
Sikorsky-Rittenhouse*	-68.4	109.5	270	1 ring	(6)	66 ± 9
Orientale-Southwest**	-28.2	251.1	276	1 ring	(6)	173 ± 29
Harkhebi	40.0	98.6	280	1 ring	(6)	106 ± 29
Aestuum**	11.2	351.0	310	1 ring	(28)	252 ± 10
Ingenii	-32.8	163.8	342	1 ring	(6)	183 ± 19
Amundsen-Ganswindt*	-81	123.0	378	1 ring	(6)	273 ± 46
Crüger-Sirsalis*	-16.0	293.0	{430}	Inner ring 212 km	(6, 29)	334 ± 20
Dirichlet-Jackson*	13.4	201.8	{440}	1 ring	(29, *54*)	186 ± 22
Moscoviense North**‡	27.2	148.8	640	1 ring	(6)	620 ± 101
Nubium*	-21.3	343.4	[690]	1 ring	(*5*)	82 ± 41

South Pole-Aitken*	-53.0	191.1	2400	1 ring	(*53*)	395[§]

[‡] This basin is an older basin onto which the peak-ring basin Moscoviense was emplaced. Its main ring has been proposed to be the outer ring of Moscoviense; however, gravity data and morphology suggest that these rings represent two separate impact basins (e.g., *41*).

[§]The Bouguer anomaly contrast for the South Pole-Aitken basin was estimated from a bandpassed solution from spherical harmonic degree 1 to 540, but the structure is not considered a peak-ring-like basin because of its size.

Table S6. Lunar depressions suggested by GRAIL data to be degraded basins. These features lack confidently measurable topographic rings but are confirmed in this study. Provisional names assigned here: TOPO and CTA are from Frey (*28*), Fitzgerald-Jackson and Fowler-Charlier are from Cook et al. (*29*). Diameters are estimated on the basis of Bouguer gravity anomaly highs and lows, as well as azimuthally averaged topographic relief. The main ring diameter of Asperitatis is estimated on the basis of incomplete outer ring remnants and is set to twice that of the inner topographic ring enclosing the positive Bouguer anomaly. Mutus-Vlacq (*5*) is a broad depression with an elliptical positive Bouguer anomaly encircled halfway by a negative annulus. The Lamont depression within Mare Tranquilitatis exhibits a 72-km-diameter ghost ring and a substantial positive Bouguer anomaly, for which the scaling relationship in Fig. 3 would imply a main ring diameter of 370 km. Lamont otherwise lacks discernible basin structure, and its depression lies along a north–south- trending linear anomaly associated with the Procellarum region, interpreted as a frozen remnant of the regional magmatic plumbing system (57), making its identification uncertain. Positive circular Bouguer anomaly features in Procellarum with neutral or positive relief that are associated with volcanic areas such as Aristarchus and Marius domes are not considered basins (next table).

Name	Latitude (°N)	Longitude (°E)	Main ring diameter (km)	Inner ring diameter (km)	Bouguer anomaly contrast (mGal)	Note
Szilard North	34.3	105.6	{200}		182 ± 20	encloses crater Szilard
Copernicus-H	7.2	341.8	{210}		162 ± 5	flooded crater; Fig. S6
TOPO-13	-37.25	147.4	[220]		103 ± 12	smaller, incomplete rim
Bartels-Voskresenskiy	27.6	268.2	[290]	[160]	197 ± 22	Fig. S5 with Lorentz
Medii	1.1	0.6	[326]		160 ± 8	CTA-01
Fowler-Charlier	39.2	218	[374]		156 ± 18	Fig. S14
Vaporum	14.2	3.1	{410}	205	120 ± 24	CTA-02
Lamont	4.8	23.4	[370]	[72]	213 ± 23	Fig. S1
Serenitatis North	35.8	17.0	[420]	{210}	161 ± 26	Fig. S1
Crisium East	16.7	66.0	{372}	{186]	339 ± 45	TOPO-05, Fig. S10
Mutus-Vlacq	-53.5	24.0	{450}	{225}	107 ± 13	depression
TOPO-22	49.4	179.0	{500}	{250}	274 ± 21	Fig. S17
Fitzgerald-Jackson	25.1	190.5	[566]	{341}	224 ± 48	Fig. S2
Fecunditatis	-4.6	52.0	[690]	{345}	205 ± 46	mare basin
Asperitatis	-7.7	26.8	{730}	[365]	260 ± 26	Fig. S4
Australe North	-35.5	96.0	{880}		103 ± 22	mare Australe, Fig. S18

Table S7. Features in basin catalogs not meeting criteria for inclusion in this study. Names given are from the referenced catalogs (see reference column). Latitudes and longitudes are from the tables in the referenced catalogs. Listed references are Wilhelms (1987)(*5*), Tables 4.1 and 4.2; Cook et al. (2000)(*54*), Table 2; Frey (2011) (*28*), Table 1; Byrne (2012) (*55*). Basin certainty and morphological designations as given in previous catalogs: Wilhelms (1987) (*5*), Tables 4.1 and 4.2; Pike and Spudis (1987) (*43*), Table 1; Frey (2011) (*28*), Tables 1 and 2. Schrödinger-Zeeman is observed to only have only one ring in LOLA data and little gravity signature, which precludes its listing in Table S4.

Name	Latitude (°N)	Longitude (°E)	Reference	Morphology	Wilhelms (1987)	Pike and Spudis (1987)	Frey (2011)
Lomonosov-Fleming	19.00	105.00	Wilhelms (1987)	depression	probable, 1 ring	not in catalog	possible, 1 ring
Tranquilitatis	7.00	30.00	Wilhelms (1987)	partially elevated mare region	probable, 1 ring	not in catalog	no topographic basin, Table 1
Australe	-51.50	94.50	Wilhelms (1987)	mare-filled depressions	definite, 3 rings	not in catalog	no topographic basin, Table 1
Al-Khwarizmi-King	1.00	112.00	Wilhelms (1987)	no depression/rings	doubtful, 1 ring	not in catalog	no topographic basin, Table 1
Pingré-Hausen	-56.00	278.00	Wilhelms (1987)	depression	possible, 1 ring	not in catalog	no topographic basin, Table 1
Werner-Airy	-24.00	12.00	Wilhelms (1987)	no depression/rings	doubtful, 1 ring	not in catalog	no topographic basin, Table 1
Flamsteed-Billy	-7.50	315.00	Wilhelms (1987)	no depression/rings	possible, 1 ring	not in catalog	no topographic basin, Table 1
Marginis	20.00	84.00	Wilhelms (1987)	no depression/rings	possible, 1 ring	not in catalog	no topographic basin, Table 1
Insularum	9.00	342.00	Wilhelms (1987)	no depression/rings	possible, 1 ring	not in catalog	no topographic basin, Table 1
Grissom-White	-44.00	199.00	Wilhelms (1987)	no depression/rings	possible, 1 ring	not in catalog	no topographic basin, Table 1
Tsiolkovsky-Stark	-15.00	128.00	Wilhelms (1987)	no depression/rings	indistinct, 1 ring	not in catalog	not in catalog, excluded
Keeler-Heaviside	-10.00	162.00	Wilhelms (1987)	overlapping craters	definite, 2 rings	multiring basin	not in catalog, excluded
Bailly-Newton	-73.00	303.00	Cook et al. (2000)	no depression/rings	not in catalog	not in catalog	not in catalog
Schrödinger-Zeeman	-80.8	191.00	Cook et al. (2000)	1 ring (166 km)	not in catalog	not in catalog	not in catalog
Sylvester-Nansen	83.00	45.00	Cook et al. (2000)	depression	not in catalog	not in catalog	not in catalog
Chaplygin-Mandelstaam	9	161	Byrne (2012) (or St. John-Telius)	1040-1400 km depression	not in catalog	not in catalog	not in catalog
Kohlschutter-Leonov	13	156	Cook et al (2002)	400 km depression	not in catalog	not in catalog	cf. TOPO-17
TOPO-2	-15.62	6.97	Frey et al. (2011)	depression	not in catalog	not in catalog	likely, 1 ring
TOPO-3	54.98	33.71	Frey et al. (2011)	depression	not in catalog	not in catalog	likely, 3 rings
TOPO-4	-46.88	66.98	Frey et al. (2011)	no depression/rings	not in catalog	not in catalog	likely, 3 rings
TOPO-6	-32.80	87.50	Frey et al. (2011)	depression	not in catalog	not in catalog	likely, 2 rings
TOPO-7	-34.23	98.46	Frey et al. (2011)	depression	not in catalog	not in catalog	likely, 1 ring
TOPO-8	-26.87	103.35	Frey et al. (2011)	depression	not in catalog	not in catalog	likely, 3 rings
TOPO-9	-50.80	116.67	Frey et al. (2011)	depression	not in catalog	not in catalog	likely, 3 rings
TOPO-10	57.80	117.40	Frey et al. (2011)	no depression/rings	not in catalog	not in catalog	likely, 3 rings
TOPO-11	50.14	124.74	Frey et al. (2011)	no depression/rings	not in catalog	not in catalog	likely, 2 rings
TOPO-12	-16.34	138.77	Frey et al. (2011)	no depression/rings	not in catalog	not in catalog	likely, 1 ring
TOPO-14	-5.52	149.64	Head et al.(2010); Frey et al. (2011)	depression, 0 Bouguer	not in catalog	not in catalog	likely, 2 rings
TOPO-15	-64.80	150.29	Frey et al. (2011)	depression	not in catalog	not in catalog	likely, 1 ring
TOPO-17	14.43	156.46	Frey et al. (2011);	600 km depression	not in catalog	not in catalog	likely, 3 rings

TOPO-18	-19.18	160.94	Frey et al. (2011)	depression	not in catalog	not in catalog	likely, 3 rings
TOPO-19	-0.19	170.74	Head et al.(2010); Frey et al. (2011)	elevated region with + Bouguer	not in catalog	not in catalog	likely, 2 rings
TOPO-20	39.61	176.43	Frey et al. (2011)	no depression/rings	not in catalog	not in catalog	likely, 1 ring
TOPO-21	-71.56	177.77	Frey et al. (2011)	depression	not in catalog	not in catalog	possible, 3 rings
TOPO-23	-57.08	197.90	Frey et al. (2011)	depression	not in catalog	not in catalog	likely, 3 rings
TOPO-25	-57.44	222.70	Frey et al. (2011)	depression	not in catalog	not in catalog	possible, 1 ring
TOPO-26	-14.89	240.77	Frey et al. (2011)	no depression/rings	not in catalog	not in catalog	possible, 1 ring
TOPO-27	-10.42	243.78	Frey et al. (2011)	no depression/rings	not in catalog	not in catalog	possible, 1 ring
TOPO-28	29.58	245.74	Frey et al. (2011)	depression	not in catalog	not in catalog	likely, 3 rings
TOPO-31	42.06	294.45	Frey et al. (2011)	depression	not in catalog	not in catalog	likely, 3 rings
TOPO-32	20.45	297.86	Frey et al. (2011)	depression	not in catalog	not in catalog	likely, 3 rings
TOPO-33	-38.15	298.04	Frey et al. (2011)	depression	not in catalog	not in catalog	likely, 1 ring
TOPO-34	-43.98	303.81	Frey et al. (2011)	no depression/rings	not in catalog	not in catalog	likely, 1 ring
TOPO-35	-7.66	322.19	Frey et al. (2011)	depression	not in catalog	not in catalog	likely, 2 rings
TOPO-37	59.16	337.71	Frey et al. (2011)	depression	not in catalog	not in catalog	likely, 3 rings
TOPO-38	37.85	341.23	Frey et al. (2011)	Imbrium inner ring	not in catalog	not in catalog	likely, 1 ring
TOPO-40	15.76	347.45	Frey et al. (2011)	no depression/rings	not in catalog	not in catalog	likely, 1 ring
CTA-3	-24.58	4.27	Frey et al. (2011)	no depression/rings	not in catalog	not in catalog	likely, 1 ring
CTA-4	-83.37	32.90	Frey et al. (2011)	no depression/rings	not in catalog	not in catalog	possible, 1 ring
CTA-5	42.30	70.45	Frey et al. (2011)	depression	not in catalog	not in catalog	likely, 1 ring
CTA-6	29.08	80.50	Frey et al. (2011)	depression	not in catalog	not in catalog	likely, 2 rings
CTA-7	47.50	95.78	Frey et al. (2011)	no depression/rings	not in catalog	not in catalog	likely, 1 ring
CTA-8	19.89	106.78	Frey et al. (2011)	depression	not in catalog	not in catalog	likely, 3 rings
CTA-9	23.18	118.19	Frey et al. (2011)	no depression/rings	not in catalog	not in catalog	likely, 1 ring
CTA-10	-25.20	122.34	Frey et al. (2011)	no depression/rings	not in catalog	not in catalog	likely, 1 ring
CTA-11	27.08	127.88	Frey et al. (2011)	no depression/rings	not in catalog	not in catalog	likely, 2 rings
CTA-12	-36.82	128.62	Frey et al. (2011)	no depression/rings	not in catalog	not in catalog	likely, 2 rings
CTA-13	15.91	135.13	Frey et al. (2011)	no depression/rings	not in catalog	not in catalog	likely, 1 ring
CTA-14	76.61	142.57	Frey et al. (2011)	no depression/rings	not in catalog	not in catalog	likely, 2 rings
CTA-26	26.51	188.52	Frey et al. (2011)	no depression/rings	not in catalog	not in catalog	likely, 2 rings
CTA-15	-15.34	190.61	Frey et al. (2011)	no depression/rings	not in catalog	not in catalog	likely, 3 rings
CTA-16	50.79	195.51	Frey et al. (2011)	no depression/rings	not in catalog	not in catalog	likely, 1 ring
CTA-17	40.11	210.85	Frey et al. (2011)	depression	not in catalog	not in catalog	likely, 1 ring
CTA-18	18.60	236.62	Frey et al. (2011)	no depression/rings	not in catalog	not in catalog	likely, 1 ring
CTA-19	-34.66	245.75	Frey et al. (2011)	no depression/rings	not in catalog	not in catalog	likely, 2 rings
CTA-20	67.75	247.52	Frey et al. (2011)	depression	not in catalog	not in catalog	possible, 1 ring
CTA-21	61.89	285.96	Frey et al. (2011)	depression	not in catalog	not in catalog	likely, 2 rings
CTA-22	1.83	299.75	Frey et al. (2011)	depression	not in catalog	not in catalog	likely, 1 ring
CTA-23	12.58	306.65	Frey et al. (2011)	no depression/rings	not in catalog	not in catalog	possible, 1 ring
CTA-24	0.37	314.68	Frey et al. (2011)	no depression/ring	not in catalog	not in catalog	likely, 1 ring
CTA-27	18.42	341.56	Frey et al. (2011)	depression	not in catalog	not in catalog	likely, 2 rings